

THE INFLUENCE OF BLADE PROPERTIES ON THE FORCED RESPONSE OF MISTUNED BLADED DISKS

Andreas Hohl*

Institute of Dynamics and Vibration Research
Leibniz Universität Hannover
Appelstraße 11
30167 Hannover, Germany
hohl@ids.uni-hannover.de

Benedikt Kriegesmann

Institute for Structural Analysis
Leibniz Universität Hannover
Appelstraße 9a
30167 Hannover, Germany
b.kriegesmann@ids.uni-hannover.de

Jörg Wallaschek, Lars Panning

Institute of Dynamics and Vibration Research
Leibniz Universität Hannover
Appelstraße 11
30167 Hannover, Germany
wallaschek@ids.uni-hannover.de
panning@ids.uni-hannover.de

ABSTRACT

In turbomachinery applications bladed disks are subjected to high dynamic loads due to fluctuating gas forces. Dynamic excitation can result in high vibration amplitudes which can lead to high cycle fatigue (HCF) failures. Herein, the blades are almost identical but differ due to wear or small manufacturing tolerances. Especially, after regeneration and repair procedures the properties of the blades can differ with a high variance. These deviations of the blade properties can lead to a localization of the vibrational energy in single blades and even higher risk of HCF. A recently developed substructure model with a combination of the Hurty transformation or Component Mode Synthesis (CMS) and the so called Wave Based Substructuring (WBS) is used to obtain a Reduced Order Model (ROM) with a reasonable low number of degrees of freedom. The CMS of the disk can be calculated with one cyclic disk segment of the underlying finite element model. The WBS is used to describe the numerous coupling degrees of freedom between the disk and the blades with a truncated set of waves. The orthogonal waves are derived by a Singular Value Decomposition or a QR decomposition from the coupling nodes normal modes calculated by a cyclic modal analysis of the full structure. The blade eigenvalues of the clamped blade can be mistuned individually under consideration of the variance as well as the correlation between the different eigenvalues of the blades. Monte-Carlo-Simulations are performed to calculate the effect of these parameters on the forced response

of a mistuned bladed disk for blade dominated modes. Furthermore, Monte-Carlo-Simulations and a constraint optimization approach is used to calculate the worst and best case blade patterns for specific blade patterns and blade patterns with distributed blade properties.

INTRODUCTION

Bladings in turbomachinery applications are subjected to high dynamic loads due to fluctuating gas or steam forces. The high stresses during operation cause a need for a regular regeneration e.g. of an aero engine. The maintenance and overhaul cost are amongst others caused by the reparation of the blades, especially if new parts are needed. Furthermore, the reduction of maintenance costs is a major chance to reduce costs of operations of a jet engine [1]. Therefore, methods are needed to reduce the contingent of new parts and determine the tolerances for regenerated blades.

The blisk or bladed disk is often assumed to be cyclic symmetric but differs due to wear or small manufacturing tolerances or the overhaul procedure of the blades in real applications. These small deviations of the blade properties can lead to a localization of the vibrational energy to single blades, see e.g. [2] and [3]. Therefore, this effect called mistuning can increase the risk of HCF failures.

For practical blisks spatial finite element models are essential to calculate the stresses of blades during the operation of the

*Address all correspondence to this author.

turbine. Finite element models of real bladed disks have up to 10^7 DOF per segment. Therefore, reduction techniques are employed to reduce the number of degrees of freedom of the blisk. The common techniques can basically be divided into Component Mode-based methods and System-Mode-based methods. A general overview of these methods used for the reduction of bladed disks is given in [4]. The benefit of the CMS method is that mistuning can be modeled directly with distributed individual (fixed interface) blade eigenfrequencies. These are usually measured in bench tests and therefore suitable for the CMS method. Furthermore, with a suitable number of ansatz functions, e.g. component modes, the agreement with the finite element model concerning the analysis of dynamic effects is generally very good [5]. A disadvantage is the numerous interface degrees of freedom (DOF) between the substructures and still rather large reduced order models. To overcome the numerous interface degrees of freedom a second modal reduction can be applied to the CMS model, see e.g. [6]. Furthermore, a cyclic approach to calculate the CMS of the disk has been presented in [6].

In this paper, a Component Mode-based method to model the blisk is presented with a cyclic calculation of the substructure of the disk, see [7] and [8]. With the recently developed Wave Based Substructuring [9] the models based on the CMS can be further reduced with a description of the interface nodes between two substructures with so called waves derived from the mode shapes of the whole structure at the coupling degrees of freedom calculated with a singular-value decomposition. The waves are orthogonal and have a contribution of all considered mode shapes. Mode shapes of the whole system as a reduced basis have first been used in [10] to reduce the coupling degrees of freedom, where loaded interface modes were applied. These ansatz functions are generally not orthogonal. Since the parts of the mode shapes at the coupling degrees of freedom for a family of modes are very similar, this can lead to a redundant choice of ansatz functions. Because of the substructuring, the mistuning can be directly applied to the blades' density, Young's modulus or eigenfrequencies. In the latter case, the variance between the different blades and the correlation between the eigenvalues or modal masses of different mode shapes are considered in this paper. The method is restricted to small mistuning, since component mode shapes perturbations cannot be accounted for. Nevertheless, unique blades with large geometric mistuning could be inserted into the model with little effort. The applicability of this approach is shown by a calculation of worst or best case blade patterns and frequency response functions.

MODELING

Equation of Motion (EOM)

The EOM for the forced vibrations of a mistuned bladed disk with N segments is derived in this section. The inclusion of the

mistuning effects in the forced response analysis requires a dynamic model for the full bladed disk, i. e. the well-known cyclic symmetry constraints [11] cannot be used to reduce the dynamic model to just a single segment of the bladed disk or blisk. In Fig. 1, a finite element model of a full bladed disk is shown. In the following, it is assumed that the bladed disk can be treated as a linear elastic structure. Applying the Finite Element Method (FEM), the forced response of the full bladed disk can be computed by

$$[-\omega_e^2 \mathbf{M} + i\omega_e \mathbf{C} + (1 + id_0)\mathbf{K}] \hat{\mathbf{u}} = \hat{\mathbf{f}} \quad (1)$$

using the complex notation in the frequency domain and assuming harmonic excitation and response. The EOM given in Eq. (1) is formulated in a coordinate system fixed to the rotor. The real and symmetric matrices \mathbf{M} , \mathbf{C} and \mathbf{K} denote the mass, the viscous material damping and the stiffness matrix and the vector $\hat{\mathbf{u}}$ the complex nodal displacement amplitudes. A structural damping can be modeled in terms of the structural loss factor d_0 . On the right-hand-side of Eq. (1), the vector $\hat{\mathbf{f}}$ represents the complex excitation force amplitudes acting on the airfoils of the blades, ω_e denotes the associated excitation frequency. The EOM is formulated in a rotating, i. e. non-inertial, frame of reference fixed to the rotor spinning with the constant angular velocity ω_r , see Fig. 1. Therefore, the stiffness matrix \mathbf{K} generally includes terms accounting for the rotational effects in addition to the elastic stiffness matrix \mathbf{K}_e . These additional terms consist of a geometric stiffness matrix $\mathbf{K}_g(\omega_r)$ describing the stiffening effect of the centrifugal forces and a spin-softening matrix $\mathbf{K}_{s,m} = -\omega_r^2 \mathbf{M}_{s,m}$ describing the stiffness softening due to the changing direction of the centrifugal forces [12]. Note that the mass matrix \mathbf{M} is not identical to the spin-softening mass matrix \mathbf{M}_m . It is also possible to include a skew-symmetric gyroscopic matrix \mathbf{G} in the EOM in order to consider the Coriolis forces.

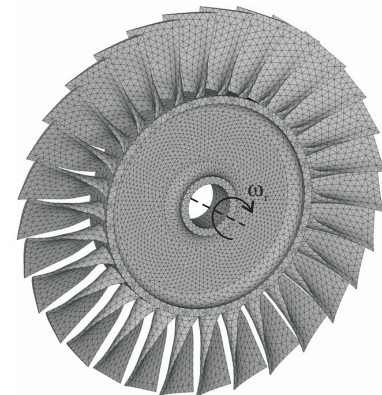


FIGURE 1. FINITE ELEMENT MODEL OF A FULL BLADED DISK

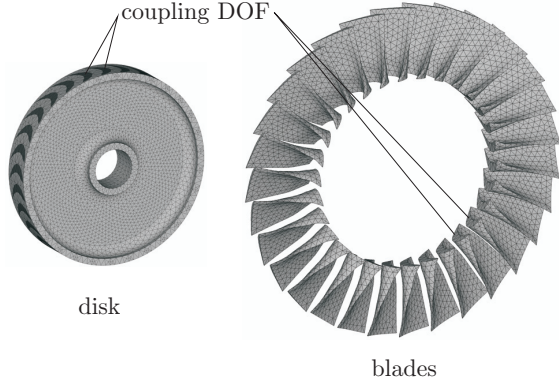


FIGURE 2. FINITE ELEMENT MODELS OF THE SUBSTRUCTURES OF THE DISK AND THE BLADES AND THE COUPLING DEGREES OF FREEDOM.

Additionally, aerodynamic coupling can have a major contribution to the forced response of blisks, in particular if the structural coupling between the adjacent blades is small. This is because the blade amplitudes are very sensitive to changes in the overall stiffness or damping. This contribution is not considered yet, but could be implemented if the aerodynamic stiffness and damping matrix would be determined, e.g. with an approach similar to the one proposed in [13]. In the forced response analysis of the mistuned bladed disk it is assumed that the excitation corresponds to a so-called engine order type excitation with EO nodal diameters resulting in a harmonic excitation force vector. Thus, the excitation forces acting on the N airfoils can be expressed by

$$\mathbf{f}(t) = \Re \left\{ \hat{\mathbf{f}} e^{i\omega_e t} \right\} = \Re \left\{ \begin{bmatrix} (1)\hat{\mathbf{f}} \\ (2)\hat{\mathbf{f}} \\ \vdots \\ (N)\hat{\mathbf{f}} \end{bmatrix} e^{i\omega_e t} \right\} \quad (2)$$

with the following relation between the excitation force amplitudes acting on the first and on the h -th airfoil

$${}^{(h)}\hat{\mathbf{f}} = e^{-i(h-1)\Delta\varphi} {}^{(1)}\hat{\mathbf{f}} \quad \text{for } h = 1(1)N \quad (3)$$

using the angular excitation frequency defined as $\omega_e = EO \omega_r$ and the interblade phase angle $\Delta\varphi = EO \frac{2\pi}{N}$.

According to [14], finite element models of real bladed disks have up to 10^7 DOF. Therefore, the forced response calculation requires a reduced order model (ROM). The reduction technique used in the analysis of mistuned bladed disks is based on the CMS technique and is presented in the following section.

Component Mode Synthesis of the Blades

The whole bladed disk is divided into the substructures of the disk and the N blades, Fig. 2. In particular, the common substructure method of Craig and Bampton [15] is used. The structural matrices α_b of the blades are partitioned into master or coupling (m) and slave (s) degrees of freedom:

$$\alpha_b = \begin{bmatrix} \alpha_{mm} & \alpha_{ms} \\ \alpha_{sm} & \alpha_{ss} \end{bmatrix}_b \quad \text{for } \alpha = \mathbf{K}, \mathbf{C}, \mathbf{M} \quad (4)$$

The displacement vector $\hat{\mathbf{u}}_b$ of a single blade can be expressed with the CMS transformation matrix \mathbf{T}_b as

$$\hat{\mathbf{u}}_b = \begin{bmatrix} \hat{\mathbf{u}}_{b,m} \\ \hat{\mathbf{u}}_{b,s} \end{bmatrix} = \begin{bmatrix} \mathbf{I} & \mathbf{0} \\ \Psi_b & \Phi_b \end{bmatrix} \begin{bmatrix} \hat{\mathbf{u}}_{b,m} \\ \hat{\boldsymbol{\eta}}_b \end{bmatrix} = \mathbf{T}_b \begin{bmatrix} \hat{\mathbf{u}}_{b,m} \\ \hat{\boldsymbol{\eta}}_b \end{bmatrix}. \quad (5)$$

Herein, Ψ_b are the so called constraint modes, which describe the displacement of the slave degrees of freedom due to a unit displacement of a single master degree of freedom. These are derived by

$$\Psi_b = -\mathbf{K}_{b,ss}^{-1} \mathbf{K}_{b,sm}. \quad (6)$$

The second type of ansatz functions is a truncated set Φ_b of cantilevered blade mode shapes. These are derived by a modal analysis of the slave degrees of freedom only (fixed master degrees of freedom):

$$\mathbf{K}_{b,ss} \Phi_b = \mathbf{M}_{b,ss} \Phi_b \Lambda_b \quad (7)$$

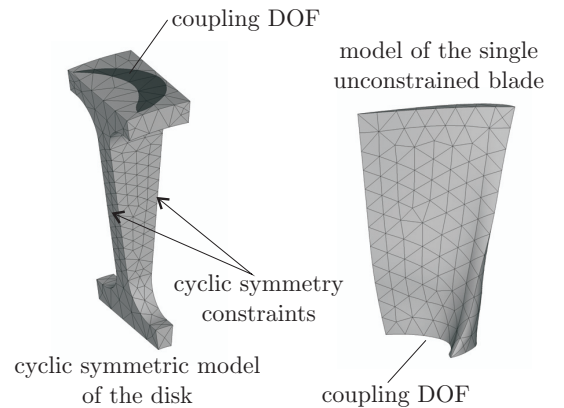


FIGURE 3. DISK SEGMENT WITH CYCLIC SYMMETRY CONSTRAINTS AND BLADE SUBSTRUCTURE.

The reduction of the blade's structural matrices is then achieved by

$$\alpha_{\text{red},b} = \mathbf{T}_b^T \alpha_b \mathbf{T}_b \quad \text{for } \alpha = \mathbf{K}, \mathbf{C}, \mathbf{M}. \quad (8)$$

Note that the reduced stiffness matrix $\mathbf{K}_{\text{red},b}$ contains as a submatrix the squares of the regular eigenfrequencies Λ_b of the mass normalized cantilevered blade mode shapes.

Component Mode Synthesis of the Disk

The CMS of the disk is calculated from the system matrices α_{seg} ($\alpha = \mathbf{K}, \mathbf{C}, \mathbf{M}$) of one disk segment. In cyclic symmetric structures the complex mode shapes of the system can be described by forward and backward traveling waves, [11]. The constant phase shift $\Delta\varphi_k = 2\pi k/N$ between the left and the right side of one cyclic segment depends on the nodal diameter ND or harmonic index $k = 0(1)N - 1$ of the mode shape, Fig. 3. Utilizing the transformation matrix $\hat{\mathbf{T}}_k$ the complex amplitudes $\hat{\mathbf{u}}_{\text{seg}}$ of one cyclic disk segment (corresponding to the whole disk) can be calculated by

$$\hat{\mathbf{u}}_{\text{seg}} = \begin{bmatrix} \hat{\mathbf{u}}_{d,L} \\ \hat{\mathbf{u}}_{d,I} \\ \hat{\mathbf{u}}_{d,R} \end{bmatrix} = \underbrace{\begin{bmatrix} \mathbf{0} & e^{-i\frac{2\pi k}{N}} \mathbf{A} \\ \mathbf{I} & \mathbf{0} \\ \mathbf{0} & \mathbf{I} \end{bmatrix}}_{\hat{\mathbf{T}}_k} \begin{bmatrix} \hat{\mathbf{u}}_{d,I} \\ \hat{\mathbf{u}}_{d,R} \end{bmatrix}. \quad (9)$$

Thereby, the complex amplitudes $\hat{\mathbf{u}}_{d,L}$ at the left side can be substituted by the complex amplitudes $\hat{\mathbf{u}}_{d,R}$ at the right side of the disk segment with a phase shift $\Delta\varphi_k$ and a rotation of the cartesian coordinates with the pitch angle $\Delta\varphi = 2\pi/N$. \mathbf{A} denotes the corresponding rotation matrix. The amplitudes $\hat{\mathbf{u}}_{d,I}$ inside the disk segment remain unchanged. The cyclic system matrices are then derived by

$$\hat{\alpha}_{d,k} = \hat{\mathbf{T}}_k^H \alpha_{\text{seg}} \hat{\mathbf{T}}_k \quad \text{with } \alpha = \mathbf{K}, \mathbf{C}, \mathbf{M} \quad (10)$$

for every harmonic index k . Thereby, the superscript ^H denotes the Hermitian or complex conjugate transpose. Rearranging the degrees of freedom in master (index m) and slave (index s) degrees of freedom the complex Component Mode Synthesis $\hat{\alpha}_{d,\text{cms},k}$ of the system matrices can be calculated analogous to Eqs. (6)-(8) for every harmonic index k , respectively. The system matrix of the whole disk can be derived using the theory of block diagonal matrices. For that purpose, the cyclic matrices are arranged diagonally and the physical degrees of freedom can be expanded using the fourier matrix

$$\hat{\mathbf{F}} = [\hat{f}_{mn}] \quad \text{with } \hat{f}_{mn} = \frac{1}{\sqrt{N}} e^{-i(m-1)(n-1)\frac{2\pi}{N}}. \quad (11)$$

A detailed description of the procedure can be found in [8] or a similar one in [6].

CMS of the Whole System

The CMS is assembled by the N substructures of the blade and the substructure of the disk, where the constraint of equal displacements

$$\hat{\mathbf{u}}_{d,m,h} = \hat{\mathbf{u}}_{b,m,h}, \quad h = 1(1)N \quad (12)$$

at the coupling DOFs between disk and blades has to be satisfied. The structural matrices \mathbf{K}_{cms} and \mathbf{M}_{cms} can be assembled by the submatrices derived by the Component Mode Synthesis. The DOFs of the reduced system matrices are composed of the component modes η_d and $\eta_{b,h}$ of the disk and of all blades $h = 1(1)N$, respectively, and the master DOFs,

$$\hat{\mathbf{u}}_{\text{cms}} = [\hat{\boldsymbol{\eta}}^T \hat{\mathbf{u}}_m^T]^T = [\hat{\boldsymbol{\eta}}_d^T \hat{\boldsymbol{\eta}}_{b,1}^T \cdots \hat{\boldsymbol{\eta}}_{b,N}^T \hat{\mathbf{u}}_m^T]^T, \quad (13)$$

$$\hat{\mathbf{u}}_m = \hat{\mathbf{u}}_{d,m} = [\hat{\mathbf{u}}_{b,m,1}^T \hat{\mathbf{u}}_{b,m,2}^T \cdots \hat{\mathbf{u}}_{b,m,N}^T]^T. \quad (14)$$

The complex physical amplitudes $\hat{\mathbf{u}}^*$ of the whole structure can be determined by

$$\hat{\mathbf{u}}^* = \begin{bmatrix} \hat{\mathbf{u}}_s \\ \hat{\mathbf{u}}_m \end{bmatrix}^* = \underbrace{\begin{bmatrix} \Phi & \Psi \\ \mathbf{0} & \mathbf{I} \end{bmatrix}}_{\hat{\mathbf{T}}_{\text{cms}}} \begin{bmatrix} \hat{\boldsymbol{\eta}} \\ \hat{\mathbf{u}}_m \end{bmatrix}, \quad (15)$$

where $\hat{\mathbf{T}}_{\text{cms}}$ is assembled by the blockdiagonally arranged transformation matrices of the blades $\mathbf{T}_{b,h}$ with $h = 1(1)N$ and the single disk $\hat{\mathbf{T}}_d$.

$$\hat{\mathbf{T}}_{\text{cms}} = \begin{bmatrix} \hat{\Phi}_d & \mathbf{0} & \Psi_d \\ \mathbf{0} & \mathbf{bdiag}(\Phi_{b,h})_{h=1(1)N} & \mathbf{bdiag}(\Psi_{b,h})_{h=1(1)N} \\ \mathbf{0} & \mathbf{0} & \mathbf{I} \end{bmatrix} \quad (16)$$

Wave Based Substructuring

Utilizing the recently developed Wave Based Substructuring, see e.g. [9, 16], the numerous master (coupling) degrees of freedom of the substructures can be reduced. A cyclic modal analysis of the bladed disk

$$\mathbf{K}\Phi = \mathbf{M}\Phi\Lambda \quad (17)$$

with the stiffness matrix \mathbf{K} and mass matrix \mathbf{M} of the finite element model can be used to determine the transformation

$$\hat{\mathbf{u}} = \Phi \hat{\boldsymbol{\eta}} \quad (18)$$

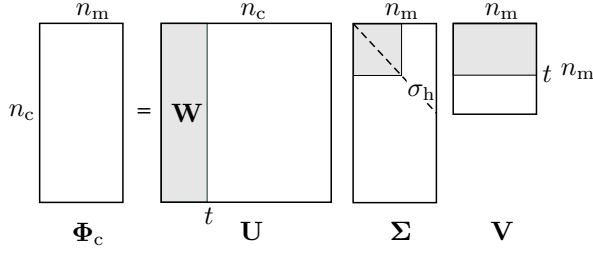


FIGURE 4. PRINCIPLE OF THE SINGULAR VALUE DECOMPOSITION. Σ IS A DIAGONAL MATRIX OF THE SQUARE ROOTS OF THE EIGENVALUES OF $\Phi_c \Phi_c^T$, \mathbf{U} CONTAINS THE EIGENVECTORS OF $\Phi_c \Phi_c^T$ AND \mathbf{V}^T CONTAINS THE EIGENVECTORS OF $\Phi_c^T \Phi_c$.

from modal coordinates $\hat{\eta}$ into physical coordinates $\hat{\mathbf{u}}$. Thereby, $\Phi_{n \times n}$ is the modal matrix which is composed of the orthogonal eigenvectors of the whole bladed disk with n degrees of freedom, which can be gained from a cyclic modal analysis. A subset $n_m < n$ of eigenvectors is selected. Furthermore, only rows corresponding to the n_c coupling degrees of freedom m are taken from the modal matrix Φ and the submatrix $\Phi_{n_m \times n_c}$ is gained. Due to the partition of the modal matrix the column vectors of $\Phi_{n_m \times n_c}$ are not orthogonal. Hence, the WBS is used to derive an orthogonal basis of the matrix $\Phi_{n_m \times n_c}$. The orthogonal basis \mathbf{U} of the columns of Φ_m can be calculated by a Singular Value Decomposition

$$\Phi_{n_m \times n_c} = \mathbf{U} \Sigma \mathbf{V}^H. \quad (19)$$

\mathbf{U} and \mathbf{V} are matrices of orthogonal ansatz functions for the rows and the columns of the modal matrix. Figure 4 depicts the principle of the singular value decomposition. Herein, Σ is a rectangular matrix and the upper diagonal submatrix contains the sorted singular values σ_h . According to [9] the contribution of the modal displacement of the coupling DOFs are dependent on the magnitude of the singular value. Hence, a limit $\frac{\sigma_h}{\sigma_1} > S$ is defined, where a typical value is $S = 10^{-6}$. The first t singular values σ_i , which satisfy this constraint, are taken from \mathbf{U} and therefore t waves

$$\mathbf{W} = \mathbf{U}_{n_m \times t} \quad (20)$$

are used. The coupling DOFs $\hat{\mathbf{u}}_m$ can be described by the complex amplitudes $\hat{\mathbf{p}}$ of the waves, that is

$$\hat{\mathbf{u}}_m = \mathbf{W} \hat{\mathbf{p}}. \quad (21)$$

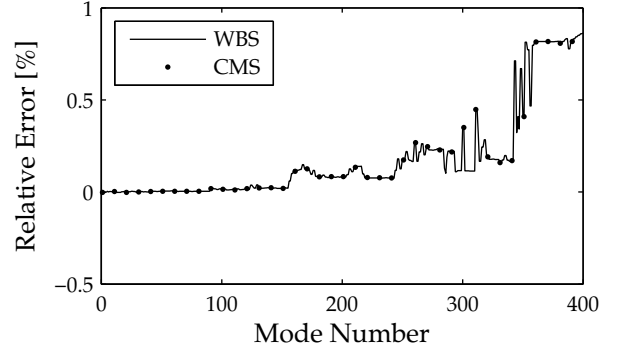


FIGURE 5. RELATIVE ERROR OF THE CMS AND WBS METHOD COMPARED TO THE FULL FINITE ELEMENT MODEL.

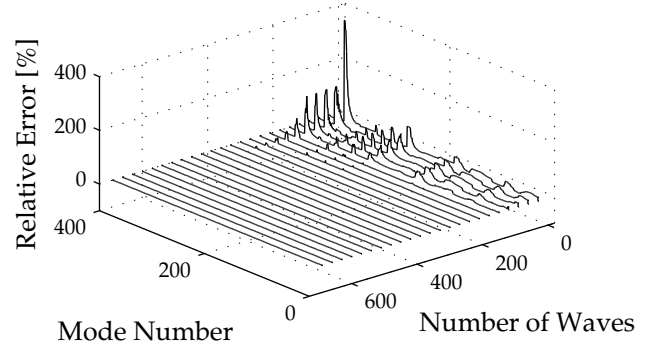


FIGURE 6. RELATIVE ERROR OF THE WBS METHOD WITH DIFFERENT NUMBERS OF WAVES COMPARED TO THE FULL FINITE ELEMENT MODEL.

The displacement vector

$$\hat{\mathbf{u}}^{**} = \begin{bmatrix} \hat{\mathbf{u}}_s \\ \hat{\mathbf{u}}_m \end{bmatrix}^{**} = \underbrace{\begin{bmatrix} \Phi & \Psi \\ \mathbf{0} & \mathbf{I} \end{bmatrix}}_{\hat{\mathbf{T}}_{\text{cms}}} \underbrace{\begin{bmatrix} \mathbf{I} & \mathbf{0} \\ \mathbf{0} & \mathbf{W} \end{bmatrix}}_{\hat{\mathbf{T}}_{\text{wbs}}} \begin{bmatrix} \hat{\eta} \\ \hat{\mathbf{p}} \end{bmatrix} \quad (22)$$

of the further reduced model can be determined by the transformation matrices $\hat{\mathbf{T}}_{\text{cms}}$ and $\hat{\mathbf{T}}_{\text{wbs}}$ of the CMS and the WBS. The CMS and the WBS have to be carried out only one time, because the mistuned mode shapes of the system can be approximated by a weighted sum of tuned component modes and waves. As mentioned above, no perturbations of blade mode shapes can be accounted for with the derived method.



FIGURE 7. FINITE ELEMENT MODEL OF A MODEL BLISK WITH 30 BLADES AND 82080 DEGREES OF FREEDOM.

Model Verification

In [7] a comparison of the FEM with the CMS and WBS substructure technique is given for the bladed disk shown in Fig. 1 and a very good agreement of the eigenvalues of the bladed disk is determined with an adequate number of component modes and waves. It is common knowledge that the CMS model converges against the full model if all component modes are considered, see e.g. [5]. The WBS method does not change the component modes of the substructure nor do the waves change the basis of the constraint modes. A theoretical set of alternative waves is the unity matrix, $\mathbf{W}^* = \mathbf{I}$, which is composed of orthogonal ansatz functions. If the number of orthogonal waves is equal to the number of physical coordinates or constraint modes the basis is equal, that is the (square) matrices \mathbf{W} and $\mathbf{W}^* = \mathbf{I}$ span the same space with the dimension of the number of constraint modes. Since the waves of the singular value decomposition are sorted by its contribution to the displacement of the mode shapes, it is possible to take a truncated set of waves with the proposed criterion. Since a full set of waves span the same space as the unity matrix, no artificial modes are expected to appear with the WBS and the method converges against the CMS.

In this numerical example, a blisk with $N = 30$ blades and 82080 degrees of freedom of the full finite element model is used, see Fig. 7. Figure 5 shows the relative error of the eigenfrequencies of the CMS and WBS against the full model. Thereby, 14 component modes of the blades and 150 component modes of the disk were considered. The number of constraint modes or master degrees of freedom is 2430 which were reduced to 700 waves. The number of degrees of freedom of the CMS and WBS is 3000 and 1270, respectively. The figure shows an exact match of the eigenfrequencies of the CMS and WBS, which supports the theoretical considerations above, and a very good agreement with the finite element model. The relative error of the eigenfrequencies of the WBS against the full model is depicted in Fig. 6 against the number of waves for the first 400 modes. With a minimum number of about 100 waves the first two families of modes

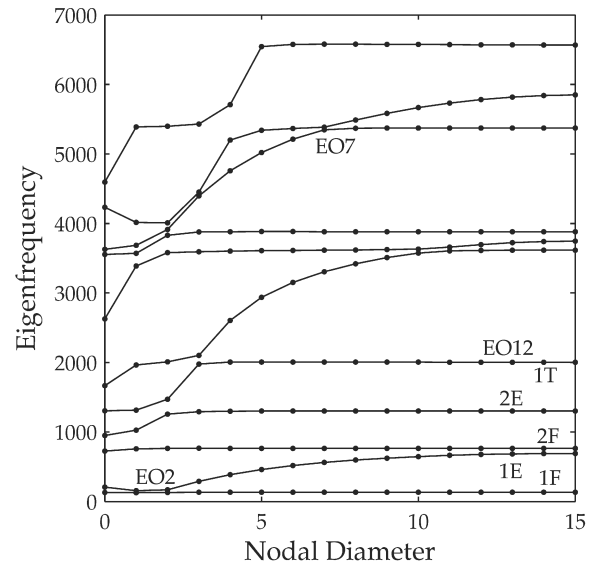


FIGURE 8. DISK SEGMENT WITH CYCLIC SYMMETRY CONSTRAINTS AND BLADE SUBSTRUCTURE.

are described properly. With an increasing number of waves the eigenfrequencies of all 400 modes are matching very well.

A nodal diameter map of the blisk is shown in Fig. 8. Frequency response functions are calculated for the worst case blade pattern ($ND = 2$), see Fig. 12. The frequency response is compared with the full model for different families of modes and engine orders, that is 1F and $EO = 2$, 1T and $EO = 12$ and the tenth family of modes with $EO = 7$, see Figs. 9-11. The frequency response is equal to the full model concerning the resonance frequencies and amplitudes for all three cases. This shows that the method works even for higher modes. If a frequency response function is calculated, a second modal reduction has been applied like proposed in [6] with an appropriate number of modes in the considered frequency range. Note that the second modal reduction has to be performed for every mistuned bladed disk. Thus, the number of degrees of freedom can then be reduced to about 30, which is the number of the modes shapes in one family of modes.

Derivation of the Mistuning of the Regenerated Blades

The eigenfrequencies of a single regenerated blade differ from the eigenfrequencies of the ideal blade due to deviations of geometry and scattering of material properties. In order to estimate the stochastic distribution of the eigenfrequencies or eigenvalues of a single blade, these parameters have to be taken into account within a probabilistic analysis. From measurements of a set of blades, the distributions of the stochastic input pa-

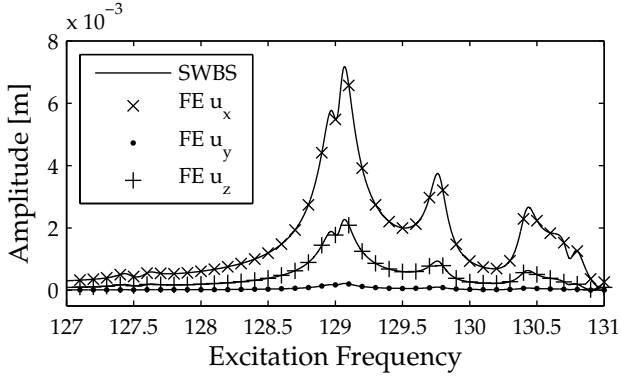


FIGURE 9. COMPARISON BETWEEN THE FINITE ELEMENT METHOD FOR A WORST CASE BLADE PATTERN FOR EO=2.

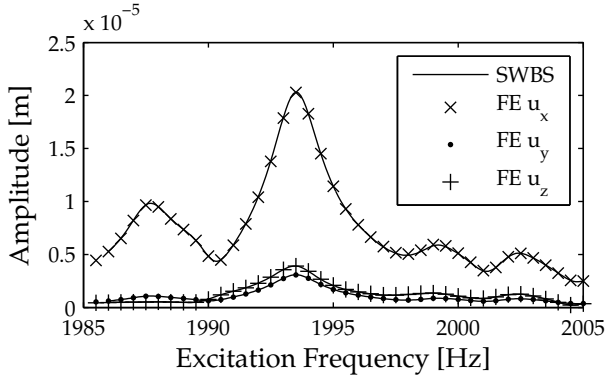


FIGURE 10. COMPARISON BETWEEN THE FINITE ELEMENT METHOD FOR A WORST CASE BLADE PATTERN FOR EO=12.

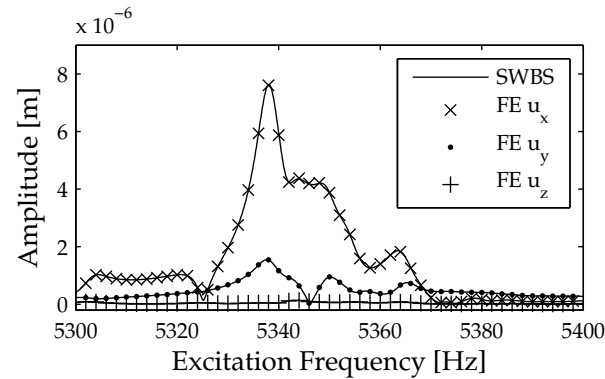


FIGURE 11. COMPARISON BETWEEN THE FINITE ELEMENT METHOD FOR A WORST CASE BLADE PATTERN FOR EO=7.

rameters can be estimated. Then, a Monte-Carlo-Simulation is performed in order to estimate the multivariate, joint distribution of the eigenfrequencies of interest, which is required for the probabilistic analysis of the whole disk. If a multi-normal distribution is assumed for the eigenfrequencies, mean vector and covariance matrix have to be determined, which can be obtained from the results of a Monte-Carlo-Simulation. However, more efficient methods than Monte-Carlo-Simulations can be used if only mean vector and covariance matrix need to be determined. One of the simplest and fastest methods is the first-order second-moment (FOSM) method, see [17]. The mean value μ_k of the k -th eigenvalue $\omega_{0,k}^2$ is estimated by

$$\mu_k \approx \omega_{0,k}^2(\mu) \quad (23)$$

where μ is the mean vector of input parameters. Assuming independence of the stochastic input parameters x_i , the variance σ_k^2 of the k -th eigenvalue $\omega_{0,k}^2$ is given by

$$\sigma_k^2 = \Sigma_{kk}^* \approx \sum_{i=1}^n \left[\left(\frac{\partial \omega_{0,k}^2}{\partial x_i} \right)^2 \text{var}(X_i) \right]. \quad (24)$$

The variances are on the diagonal of the covariance matrix Σ^* . The covariance of two eigenvalues is determined from

$$\Sigma_{kj}^* \approx \sum_{i=1}^n \left[\frac{\partial \omega_{0,k}^2}{\partial x_i}(\mu) \frac{\partial \omega_{0,j}^2}{\partial x_i}(\mu) \text{var}(X_i) \right]. \quad (25)$$

Since the functions of eigenvalues $\omega_{0,k}(\mathbf{x})$ are not given explicitly, the derivatives have to be determined numerically.

A mistuning factor δ_k is used to mistune the k -th eigenvalue of the blades. The covariance matrix and mean value have to be normated to get the mean value $E(\delta_k)$ and the covariance matrix Σ of the mistuning factor $\delta_k = \frac{\omega_{\text{mistuned},0,k}^2}{\omega_{\text{tuned},0,k}^2}$:

$$E(\delta_k) = \frac{\mu_k}{\omega_{\text{tuned},0,k}^2} \quad (26)$$

$$\Sigma_{kj} = \frac{\Sigma_{kj}^*}{\omega_{\text{tuned},0,k}^2 \omega_{\text{tuned},0,j}^2} \quad (27)$$

Implementation of the Mistuning to the Blades

In the following section a method is described to mistune the eigenvalues of the cantilevered blade modes, which are directly

accessible after the Component Mode Synthesis of the blade. Thereby, the variance of the distribution of every single eigenvalue (or modal mass) as well as the correlation between the distributions of different eigenvalues of the blades are considered. For example, the first mode shape's eigenvalue, e.g. first bending, decreases if a discrete mass is added to the top of the blade. If the torsional mode shape of the blade has a nodal line at the center of the mass, the eigenvalue will not change at all. The data of the variance of the eigenvalues and the correlation can be determined by measurements or a parametrized model of the blade as described in the prior section.

σ_k^2 and σ_j^2 are the variances of the mistuning factors of the eigenvalues k and j of a set of blades. The entry ρ_{kj} of the correlation matrix ρ contains the correlation between the distribution of the eigenvalues k and j of a set of blades. Accordingly, the diagonal entries of the matrix are equal to one. In the special cases of mistuning of the density or stiffness of the blade, all entries of the matrix ρ are equal to one. Now, the covariance matrix can be derived by

$$\Sigma_{kj} = \rho_{kj} \sqrt{\sigma_k^2 \sigma_j^2} \quad k, j = 1(1)n_m, \quad (28)$$

where n_m is the number of component modes of the blades. Alternatively, the covariance matrix can be taken from measurements or a probabilistic analysis, see Eq. (25). A Cholesky decomposition

$$\Sigma = \mathbf{R}^T \mathbf{R} \quad (29)$$

is used to calculate the mistuning factors

$$\delta_h = \mu_h + \mathbf{R}^T \mathbf{z}_h^T \quad h = 1(1)N \quad (30)$$

of the eigenvalues or modal masses of the h -th blade with the vector of the average values μ_h , whose entries are typically equal to (the multiplier) one. \mathbf{z}_h is the h -th row vector of a matrix \mathbf{Z} , whose column vectors consist of uncorrelated normally distributed entries with the mean value zero and a variance of one. A detailed description of the general procedure to calculate the correlated random numbers is described e.g. in the textbook [18].

The eigenvalues of the n_m component modes are arranged diagonally in the submatrix

$$\mathbf{K}_h = \mathbf{diag} (\omega_{hj}^2)_{j=1(1)n_m} \quad (31)$$

of a specific blade. The mistuned submatrix of the reduced stiffness matrix of the blade is then calculated with

$$\Delta_{sto,h} = \mathbf{diag} (\delta_{sto,hj})_{j=1(1)n_m} \quad (32)$$

and the matrix of the intentional mistuning

$$\Delta_{int,h} = \mathbf{diag} (\delta_{int,hj})_{j=1(1)n_m} \quad (33)$$

to

$$\mathbf{K}_{mis,h} = \Delta_{int,h} \Delta_{sto,h} \mathbf{K}_h \quad h = 1(1)N. \quad (34)$$

As an approximation, the stiffness matrix of the master or coupling degrees of freedom are mistuned with the mean value of the mistuning factors of the modal values of the specific blade h . In future works, the validity of this assumption has to be estimated.

CASE STUDY

Optimization Procedure

The methods described above can be used to calculate the forced response of a bladed disk with small blade mistuning. Since Monte-Carlo-Simulations are not suitable to calculate worst or best case blade patterns, an optimization procedure has been developed which has been proposed in [8].

The maximum resonance amplitude A_{max} , which is the maximum of the blade amplitudes of all blades in a specific excitation frequency range $\Omega_{e,min} \dots \Omega_{e,max}$ can be calculated for a specific set of parameters, namely the engine order EO , the structural damping factor d_0 and the variance of the blade pattern $VAR(\delta) = s^2$. The best case or worst case blade pattern can be calculated depending on the algebraic sign of the constraint optimization problem

$$\min \left(\mp \hat{\mathbf{u}}(VAR(\delta), [\Omega_{e,min} \dots \Omega_{e,max}], EO, d_0) \right) = \min \left(\mp \hat{\mathbf{S}}^{-1} \hat{\mathbf{f}} \right). \quad (35)$$

The constraints are

$$VAR(\delta_{sto}) = s^2 \quad (36)$$

and

$$E[\delta_{sto}] = 1, \quad (37)$$

that is the variance and the mean value of the blade pattern are constant during the procedure.

Generally, the optimization procedure works for more than one stationary point in the Campbell diagram. Thereby, two or more frequency ranges and engine orders of excitation have to be used to calculate the amplitudes, which have to be normalized to the tuned resonance amplitude. Note that even the forces on the

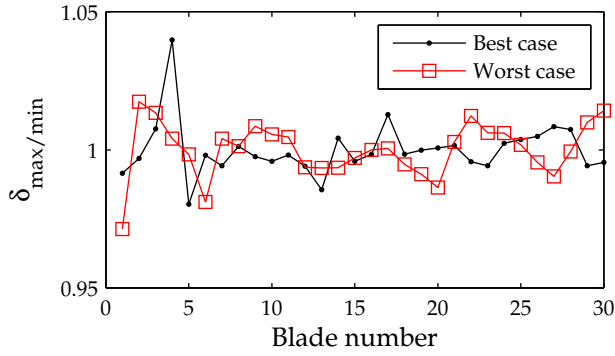


FIGURE 12. WORST AND BEST BLADE PATTERN FOR $EO = 2$ AND A VARIANCE OF $s^2 = 0.0001$.

airfoil and the system matrices might change for the mentioned different cases, e.g. due to the influence of centrifugal forces. The worst case blade pattern for more than one configuration can be determined by the maximum amplitude $A_{\max,j}$ for single configurations $j = 1(1)n_{cf}$:

$$A_{\max} = \max_{j=1(1)n_{cf}} A_{\max,j} \quad (38)$$

In case of the best case blade pattern the optimization procedure has to be used and the minimum has to be determined under consideration of two or more configurations. Nevertheless, the amplitude might not be an appropriate criterion in this case because of the mode shape dependent stresses. If the stresses cannot be determined without using a time consuming calculation with the full finite element model weighting factors for the normalized amplitudes might be a compromise.

Best Case and Worst Case Blade Patterns

The best and worst case blade patterns have been determined for $EO = 2$ and a variance of the stiffness of the $N = 30$ blades of $s^2 = 0.0001$. Note that the output of this analysis does not correspond to a specific set of blades. The structural damping factor is $d_0 = 0.001$. In Figs. 12-14 the first blade is always associated with the largest blade amplitude. Figure 13 shows the amplitudes of all blades at the resonance frequency of the blade with the highest amplitude, whereas Fig. 14 shows the maximum of all blades in the whole frequency range for both the best and worst blade pattern. In Fig. 12 the blade patterns are depicted. The amplitude amplification of the first blade is about 3 for the worst case and below 1.1 for the best case blade pattern compared to the tuned amplitude. An obvious difference is a blade with low stiffness in the worst case and a blade with high stiffness in the best case blade pattern. A case study in [8] suggests, that this is

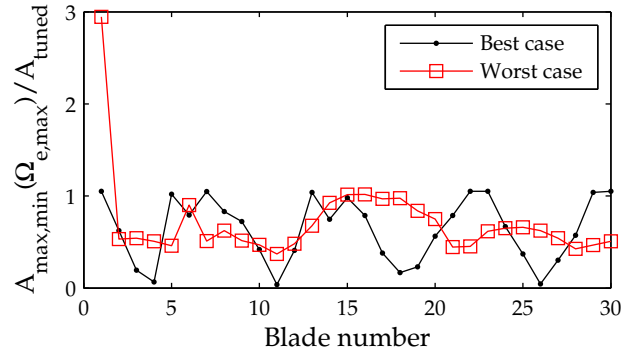


FIGURE 13. AMPLITUDES OF THE WORST AND BEST BLADE PATTERN FOR $EO = 2$ AND A VARIANCE OF $s^2 = 0.0001$ AT THE DISCRETE MAXIMUM RESPONSE EXCITATION FREQUENCY.

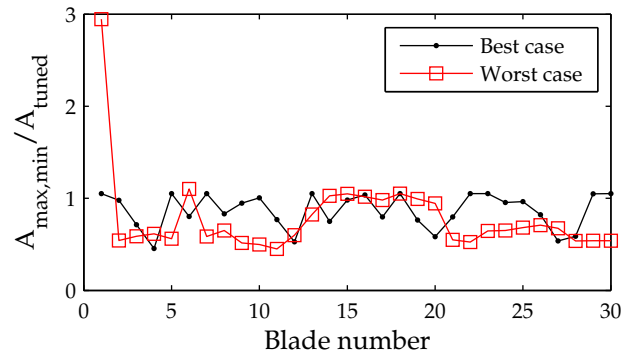


FIGURE 14. MAXIMUM AMPLITUDES OF THE WORST AND BEST BLADE PATTERN FOR $EO = 2$ AND A VARIANCE OF $s^2 = 0.0001$ DETERMINED INDEPENDENTLY FOR EVERY BLADE.

not typical regarding all engine orders of excitation. As expected, the displacement at a discrete frequency, see Fig. 13, leads to a stronger amplitude localization compared to Fig. 14. Figure 15 shows the frequency response function of the blade with the maximum blade resonance amplitude against the variance of the blade pattern from $s^2 = 0$ to $s^2 = 0.0001$. Note that the optimization procedure has been performed at $s^2 = 0.0001$. The tuned frequency response is assigned to the red line at $s^2 = 0$. The black lines mark the undamped resonance frequencies and the corresponding amplitude and an increasing frequency split of the double eigenfrequencies can be observed with a rising blade pattern variance. As mentioned above, the tuned amplitude is about one-third of the worst case blade amplitude at $s^2 = 0.0001$. The split of the eigenfrequencies corresponding to the tuned $ND = 2$ mode shapes is small compared to the best case, see Fig. 16 and the explanations below. Therefore, the resonances of both eigen-

frequencies are strongly coupled and the superposition of both resonance peaks is effective. Furthermore, both mistuned mode shapes are now localized in the worst blade, see Fig. 17. Herein, both localized mode shapes are depicted, which were calculated with the finite element model of the mistuned blisk.

In Fig. 16 the frequency response function of the best case blade pattern and the highest blade resonance amplitude is depicted against the variance of the blade pattern from $s^2 = 0$ to $s^2 = 0.0001$. The comparison of Figs. 13 and 16 shows that the eigenfrequencies split (black lines) and, therefore, the displacement of the blades is similar to a non-traveling mode shape. Be aware that a traveling mode shape is the superposition of two (real valued) mode shapes. Furthermore, as expected for a best case blade pattern, the mode shapes are not localized. Figure 18 shows the sensitivity of the best case blade pattern ($s^2 = 0.0001$) against additional stochastic mistuning $\Delta s^2 = 10^{-6}$ and $\Delta s^2 = 10^{-7}$. Probability density functions of the maximum amplitude and the underlying best case blade pattern have been calculated with 1000 Monte Carlo Simulations. As expected, the maximum amplitude rises with the variance of the additional mistuning Δs^2 . The optimization procedure is used to determine the worst case of these configurations and maximum amplitude amplifications of about 1.2 and 1.5 have been determined for $\Delta s^2 = 10^{-6}$ and $\Delta s^2 = 10^{-7}$ compared to about 1.1 for the unmodified best case. Therefore, a careful determination of the mistuning of the single blades is necessary to avoid an inaccurate prediction of the maximum resonance amplitude.

Figure 19 shows the maximum blade resonance amplitude A_{\max} subject to the logarithm of the variance s^2 of the blade pattern. The worst case resonance amplitude is rising with a declining slope (consider the logarithmic scale). In contrast, the best case resonance amplitude stays nearly constant even for high values of s^2 .

Permutations of the Worst Case Blade Pattern

In the following section the alignment of the worst case blade pattern around the disk is changed. For a specific blade pattern, since the disk is tuned,

$$n_{\text{perm}} = (N - 1)! \quad (39)$$

different alignments of the blades around the disk are possible. The goal is to determine an alignment of a unique set of blades such that the resonance amplitude or localization at specified operating points is minimized. In Fig. 20 the maximum blade amplitude A_{\max} is depicted for 2000 permutations of the worst case blade pattern ($EO = 2$, $s^2 = 0.0001$). The maximum amplitude for the same blade set differs between about $A_{\max}/A_{\text{tuned}} = 1.25$ and $A_{\max}/A_{\text{tuned}} = 3$. In conclusion the influence of the alignment of the blade set is large concerning the resonance amplitudes. Furthermore, if it is possible to chose from more than N

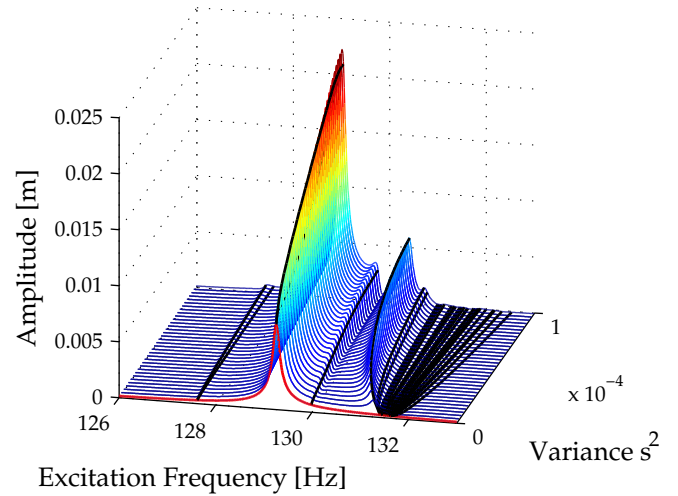


FIGURE 15. FREQUENCY RESPONSE FUNCTIONS OF THE WORST CASE BLADE PATTERN AGAINST THE VARIANCE s^2 . TUNED CASE IS DISPLAYED WITH RED LINE. UNDAMPED EIGENFREQUENCIES ARE INDICATED WITH BLACK LINES. THE FIRST FIVE EIGENFREQUENCIES ARE ASSOCIATED WITH THE TUNED $ND = 1$, $ND = 2$ AND $ND = 0$ MODE SHAPES.

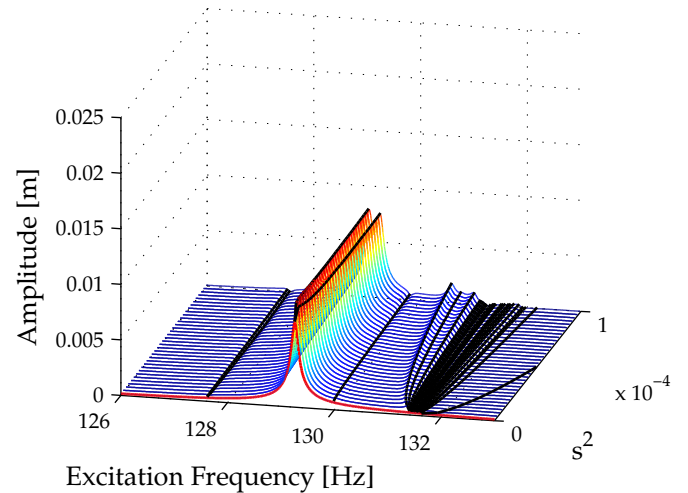


FIGURE 16. FREQUENCY RESPONSE FUNCTIONS OF THE BEST CASE BLADE PATTERN AGAINST THE VARIANCE s^2 . TUNED CASE IS DISPLAYED WITH RED LINE. UNDAMPED EIGENFREQUENCIES ARE INDICATED WITH BLACK LINES. THE FIRST FIVE EIGENFREQUENCIES ARE ASSOCIATED WITH THE TUNED $ND = 1$, $ND = 2$ AND $ND = 0$ MODE SHAPES.

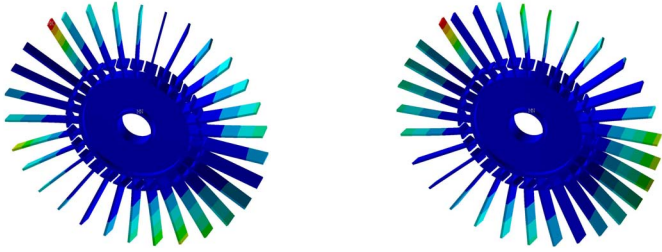


FIGURE 17. MODE SHAPES OF THE WORST CASE BLADE PATTERN ASSOCIATED WITH THE TWO TUNED $ND = 2$ MODE SHAPES.

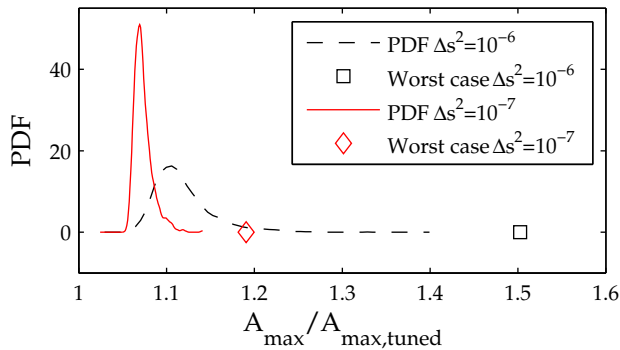


FIGURE 18. SENSITIVITY OF THE BEST CASE BLADE PATTERN ($EO=2$, $s^2 = 0.0001$) AGAINST ADDITIONAL STOCHASTICAL MISTUNING DETERMINED WITH MONTE CARLO SIMULATIONS AND THE OPTIMIZATION PROCEDURE.

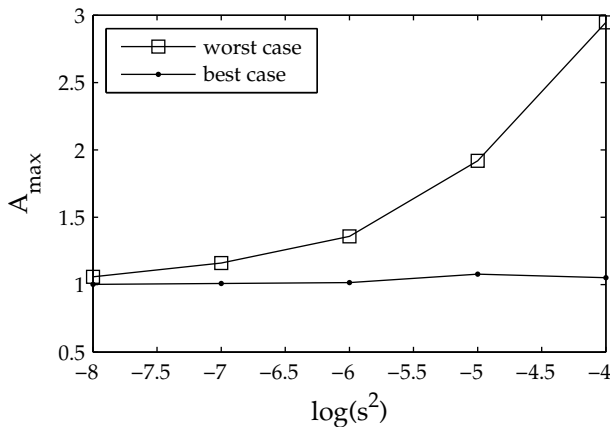


FIGURE 19. AMPLITUDES OF THE WORST AND BEST BLADE PATTERN FOR $EO=2$ FOR DIFFERENT VARIANCES s^2 .

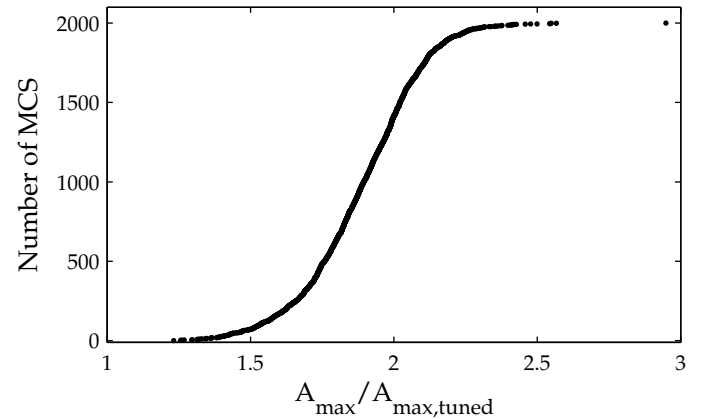


FIGURE 20. MAXIMUM RESONANCE AMPLITUDE OF 2000 PERMUTATIONS OF THE WORST CASE BLADE PATTERN.

blades, it might be possible to reduce the amplitudes to a level nearer to the tuned amplitude.

CONCLUSIONS

A method has been introduced to find an optimal alignment of a set of blades with known mistuning around the disk. Furthermore, the maximum or minimum expected amplitude can be derived with the procedure.

Therefore, a parameterized model of the blade is used to calculate the statistics of the blade eigenvalues for changes in the temperature, density, stiffness etc.. The resulting data, that is the correlation between the eigenvalues of different blade mode shapes and the variances of the eigenvalues, has been used to mistune a Component Mode-based bladed disk model.

A parameter study has been performed, where the Young's modulus of the blade has been mistuned and worst case and best case blade patterns have been determined with an optimization procedure. It has been shown that the maximum resonance amplitude of the worst case blade pattern rises subject to the variance of the stiffness mistuning, whereas the amplitudes of the best case blade pattern stay nearly constant. Further, the permutations of a worst case blade pattern can lead to far lower peak amplitudes.

This shows that the alignment of the blades around the disk can have a major impact in the expected resonance amplitude even for the same set of blades.

ACKNOWLEDGMENT

The work has been carried out within the national research project SFB 871 - Regeneration of complex goods, subproject C3 and is funded by the Deutsche Forschungsgemeinschaft (DFG).

REFERENCES

- [1] Engber, M., Klaus Rud, S. A., Gier, J., and Waschka, W., 2007. “Advanced Technologies for Next Generation Regional Jets - Survey of Research Activities at MTU Aero Engines”. *ISABE-2007-1282, MTU Aero Engines*, pp. 1–11.
- [2] Whitehead, D. S., 1966. “Effect of Mistuning on the Vibration of Turbomachine Blades Induced by Wakes”. *Journal of Mechanical Engineering Science*, **8**(1), pp. 165–186.
- [3] Ewins, D. J., 1969. “The Effects of Detuning Upon the Forced Vibrations of Bladed Disks”. *Journal of Sound and Vibration*, **9**(1), pp. 65–79.
- [4] Castanier, M. P., and Pierre, C., 2006. “Modeling and Analysis of Mistuned Bladed Disk Vibration: Status and Emerging Directions”. *Journal of Propulsion and Power*, **22**(2), pp. 384–396.
- [5] Craig, R. R., 2000. “Coupling of Substructures for Dynamic Analyses: An Overview”. In Collection of Technical Papers - AIAA/ASME/ASCE/AHS/ASC Structures, Structural Dynamics and Materials Conference 2000, pp. 1–8.
- [6] Bladh, R., Castanier, M. P., and Pierre, C., 2001. “Component-Mode-Based Reduced Order Modeling Techniques for Mistuned Bladed Disks - Part I: Theoretical Models”. *Journal of Engineering for Gas Turbines and Power*, **123**, pp. 89–99.
- [7] Hohl, A., Siewert, C., Panning, L., and Wallaschek, J., 2009. “A Substructure Based Reduced Order Model for Mistuned Bladed Disks”. *Proceedings of the ASME 2009 International Design Engineering Technical Conferences & Computers and Information in Engineering Conference (IDETC/CIE 2009)*, **2009**(48982), pp. 899–906.
- [8] Hohl, A., Panning, L., and Wallaschek, J., 2010. “Analysis of the Influence of Blade Pattern Characteristics on the Forced Response of Mistuned Blisks with a Cyclic CMS-Based Substructure Model”. *Proceedings of ASME 2010 10th Biennial Conference on Engineering Systems Design and Analysis ESDA 2010*, **2010**(49194), pp. 443–455.
- [9] Donders, S., 2008. “Computer-aided engineering methodologies for robust automotive nvh design”. Ph.d. thesis, Department of Mechanical Engineering, Division PMA, K.U. Leuven, Belgium.
- [10] Benfield, W. A., and Hrudá, R. F., 1971. “Vibration Analysis of Structures by Component Mode Substitution”. *AIAA Journal*, **9**(7), pp. 1255–1261.
- [11] Thomas, D. L., 1979. “Dynamics of Rotationally Periodic Structures”. *International Journal for Numerical Methods in Engineering*, **14**, pp. 81–102.
- [12] Cook, R. D., Malkus, D. S., Plesha, M. E., and Witt, R. J., 2002. *Concepts and Applications of Finite Element Analysis*, 4. ed. John Wiley and Sons, Chichester.
- [13] Mayorca, M. A., Vogt, D. M., Martensson, H., and Fransson, T. H., 2010. “A New Reduced Order Modeling for Stability and Forced Response Analysis of Aero-Coupled Blades Considering Various Mode Families”. *Proceedings of ASME Turbo Expo 2010: Power for Land, Sea and Air GT2010*, **2010**(44014), pp. 1209–1219.
- [14] Sternchüss, A., and Balmès, A., 2007. “Reduction of Multistage Rotor Models Using Cyclic Modeshapes”. *Proceedings of ASME Turbo Expo 2007: Power for Land, Sea and Air GT2007*, **2007**(47942), pp. 529–537.
- [15] Craig, R. R., and Bampton, M. C. C., 1968. “Coupling of Substructures for Dynamic Analyses”. *AIAA Journal*, **6**(7), pp. 1313–1319.
- [16] Donders, S., Pluymers, B., Ragnarsson, P., Hadjit, R., and Desmet, W., 2010. “The Wave-Based Substructuring Approach for the Efficient Description of Interface Dynamics in Substructuring”. *Journal of Sound and Vibration*, **329**(8), pp. 1062 – 1080.
- [17] Kriegesmann, B., Rolfes, R., Hühne, C., and Kling, A., 2010. “Probabilistic Second-Order Third-Moment Approach for Design of Axially Compressed Composite Shells”. In 51st AIAA/ASME/ASCE/AHS/ASC Structures, Structural Dynamics, and Materials Conference, pp. 1–8.
- [18] Costa, N., and Haykin, S., 2010. *Multiple-Input Multiple-Output Channel Models: Theory and Practice*, 1 ed. John Wiley & Sons, Inc., New Jersey.